

AD A102516

(12) LEVEL II

DNA 5596F

TITANIUM RESPONSE TO A NUCLEAR RADIATION ENVIRONMENT

K. Triebes

G. Liu

Acurex Corporation
Aerotherm Division
485 Clyde Avenue
Mountain View, California 94042

20 January 1981

DTIC
SELECTED
S D
AUG 6 1981
B

Final Report for Period 1 November 1979–31 October 1980

CONTRACT No. DNA 001-79-C-0158

APPROVED FOR PUBLIC RELEASE;
DISTRIBUTION UNLIMITED.

THIS WORK SPONSORED BY THE DEFENSE NUCLEAR AGENCY
UNDER RDT&E RMSS CODE B342080484 N99QAXAH12308 H2590D.

Prepared for
Director
DEFENSE NUCLEAR AGENCY
Washington, D. C. 20305

81 8 06 059

Destroy this report when it is no longer
needed. Do not return to sender.

PLEASE NOTIFY THE DEFENSE NUCLEAR AGENCY,
ATTN: STTI, WASHINGTON, D.C. 20305, IF
YOUR ADDRESS IS INCORRECT, IF YOU WISH TO
BE DELETED FROM THE DISTRIBUTION LIST, OR
IF THE ADDRESSEE IS NO LONGER EMPLOYED BY
YOUR ORGANIZATION.



UNCLASSIFIED

SECURITY CLASSIFICATION OF THIS PAGE (When Data Entered)

(19) REPORT DOCUMENTATION PAGE		READ INSTRUCTIONS BEFORE COMPLETING FORM
(18) 1. REPORT NUMBER DNA 5596F	2. GOVT ACCESSION NO.	3. REC'D TNT'S CATALOG NUMBER
4. TITLE (and Subtitle) TITANIUM RESPONSE TO A NUCLEAR RADIATION ENVIRONMENT		5. TYPE OF REPORT & PERIOD COVERED Final Report - for Period 1 Nov 79 - 31 Oct 80
6. AUTHOR(s) K. Triebes G. Liu		7. PERFORMING ORG. REPORT NUMBER FR-81-10/AS
8. PERFORMING ORGANIZATION NAME AND ADDRESS Aurex Corporation/Aerotherm Division 485 Clyde Avenue Mountain View, CA 94042		10. PROGRAM ELEMENT, PROJECT, TASK AREA & WORK UNIT NUMBERS Subtask N99QAXAH123-08
11. CONTROLLING OFFICE NAME AND ADDRESS Director Defense Nuclear Agency Washington, D.C. 20305		12. REPORT DATE 20 January 1981
13. MONITORING AGENCY NAME & ADDRESS (if different from Controlling Office)		14. NUMBER OF PAGES 42
15. DISTRIBUTION STATEMENT (of this Report)		16. SECURITY CLASS. (of this report) UNCLASSIFIED
		17a. DECLASSIFICATION/DOWNGRADING SCHEDULE N/A
17. DISTRIBUTION STATEMENT (of the abstract entered in Block 20, if different from Report)		
18. SUPPLEMENTARY NOTES This work sponsored by the Defense Nuclear Agency under RDT&E RMSS Code B342080464 N99QAXAH12308 H2590D.		
19. KEY WORDS (Continue on reverse side if necessary and identify by block number) Titanium oxidation Electron beam testing Missile shroud vulnerability		
20. ABSTRACT (Continue on reverse side if necessary and identify by block number) Titanium response under a nuclear encounter environment was modeled and incorporated into a computer program. Predictions were compared with experimental results under simulated laboratory environments. Excellent agreements were obtained for all test cases. While no evidence of sustained combustion was observed for the missile shroud under potential flight environments, it was demonstrated that titanium failed catastrophically under certain simulated conditions.		

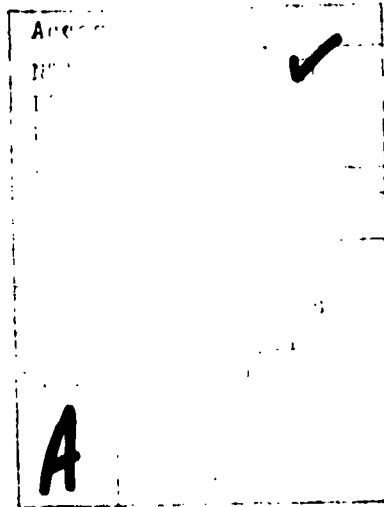
DD FORM 1 JAN 73 EDITION OF 1 NOV 68 IS OBSOLETE

UNCLASSIFIED

SECURITY CLASSIFICATION OF THIS PAGE (When Data Entered)

TABLE OF CONTENTS

<u>Section</u>		<u>Page</u>
	LIST OF ILLUSTRATIONS	2
	LIST OF TABLES	3
1	INTRODUCTION	5
	1-1 Objective	5
	1-2 Program Scope	5
2	TECHNICAL DISCUSSION	7
	2-1 Background and Simulation Requirements	7
	2-2 Combustion Model	8
	2-2.1 Titanium Oxidation Kinetics	9
	2-2.2 Model Description	10
	2-3 Computer Code of Combustion Model	13
	2-4 Simulation System and Analysis	14
3	RESULTS AND CONCLUSIONS	23
	3-1 Test Matrix and Data Summary	23
	3-2 Comparison of Analytic and Experimental Results	29
	3-3 Conclusions and Recommendations	32
4	REFERENCES	36



LIST OF ILLUSTRATIONS

<u>Figure</u>		<u>Page</u>
1	Oxidation Model and Coordinate System	11
2	Simulation Experimental Configuration	15
3	Shroud Ascent Bulk Temperature History	16
4	Predicted Oxygen Diffusion Rate to Sample Surface	17
5	Comparison of E-beam and X-ray Deposition Profiles . . .	20
6	Energy Requirements for Combustion	21
7	Postrun Photos of Tested Samples	27
8	Oscilloscope Traces for Tests 2268 and 2272	28
9	Postdeposition Temperature History of Test 2272	31
10	Predicted Temperature History of Test 2268	33
11	Predicted Temperature History of a 90 kft Nuclear Encounter	34

LIST OF TABLES

<u>Table</u>		<u>Page</u>
1	Combustion Model Constants for Ti - 6 Al - 4V	12
2	Nuclear Environment Versus Simulation Parameters	22
3	Data Summary of Test Matrix	24

BLANK PAGE

SECTION 1

INTRODUCTION

1-1 OBJECTIVE

Titanium is a candidate shroud material for advanced missile systems. Under certain conditions, titanium is known to exhibit sustained combustion, thus causing a catastrophic failure. The objective of this program was to investigate the response of titanium in a simulated upper atmosphere nuclear encounter environment. This program was a joint effort between Acurex Corporation and Physics International Company.

1-2 PROGRAM SCOPE

A combination experimental and analytical approach was adopted for this investigation. The work was performed under a two-phase program. Phase I included the design, fabrication, and checkout of experimental hardware and the acquisition of preliminary data on the titanium response to the simulated environment. An evaluation of the simulation with regard to critical encounter parameters such as material bulk temperature, oxygen diffusion rate, and pulsed deposition profile was also performed. Phase II efforts encompassed a computer modeling of the titanium surface combustion reaction and its implementation as an analytical tool for devising a comprehensive simulation test matrix. The objective was to develop a high-confidence model for the evaluation of the survivability of a titanium shroud under upper-atmosphere nuclear encounter environments. Phase I of the program has been successfully completed. The reader is referred to the Phase I final report (DNA Report 5134F, 1 Nov /9) for additional information. This report summarizes the results of the Phase II efforts undertaken by Acurex.

The Acurex program responsibility was to define the aerothermal environment, design and fabricate experimental hardware for environment simulation, assist in fielding the experiments, and model the surface

combustion reaction. Physics International provided a pulsed electron beam (e-beam) machine which simulated the nuclear energy deposition profile and performed an analysis of the pulsed radiation effects.

SECTION 2

TECHNICAL DISCUSSION

2-1 BACKGROUND AND SIMULATION REQUIREMENTS

Titanium is a candidate material for advanced missile shrouds. Because titanium may combust under the proper conditions, survivability and vulnerability assessments must be performed to determine the shroud's ability to survive a radiation threat.

During the ascent phase of the missile trajectory the shroud is heated convectively by the atmosphere. Upon exposure to a nuclear environment in the upper atmosphere, the lower energy X-rays from the burst will cause the surface scale to blow off and heat the base material leaving a fresh titanium surface at a temperature of T_{melt} , or 1,900K. Since this is above the published ignition temperature of 1,600K for titanium, sufficient oxygen availability could cause the shroud to ignite and burn. The objective of this program was to investigate the response of titanium to a nuclear environment by performing a laboratory scale experiment which simulated the conditions of an upper atmosphere nuclear encounter.

Phase I analysis of the potential environments showed that the relevant parameters that must be included in the simulation are: (1) the titanium bulk temperature caused by ascent heating, (2) surface temperature and temperature gradient caused by the nuclear energy deposition, and (3) oxygen flux through the boundary layer to the hot titanium surface. A variable pressure wind tunnel and sample heater was designed, fabricated, and calibrated to produce the required oxygen diffusion rate to the sample surface and the proper material bulk temperature. This hardware was coupled to an e-beam machine at Physics International Company to provide a pulsed radiation source. Details of

the e-beam simulation will not be given here, but are contained in a report on this project from Physics International (PI).

Prior to the test, simulation and nuclear environmental parameters were compared to determine the numerical relationship between the experiment and a projected encounter. The comparison was based on energy balance calculations which quantified the various energy loss and gain mechanisms associated with the titanium surface immediately following either X-ray or e-beam deposition. Energy is supplied to the surface by the TiO_x reaction kinetics while convection, radiation, and conduction are all loss mechanisms. Results of these preliminary calculations showed that the simulation could be considered a factor of 10 overtest when compared to a nuclear threat. The oxygen diffusion rate to the surface was higher than flight predictions resulting in increased reaction energy and the flatter e-beam deposition profile resulted in a factor of 10 lower conduction loss than was present with X-ray deposition.

Based on the above calculations it was anticipated that the titanium surface in the experiment would exhibit a brief combustion period following e-beam deposition which would last until the surface cooled below the 1,600K ignition temperature. This behavior was observed in Hi-Cam film records of the titanium sample surface. A combustion phase lasting on the order of 100 msec following e-beam deposition was recorded. The sample bulk temperature for the Phase I experiments ranged from 294 to 977K, the surface temperature following e-beam deposition was 1,900K, and the oxygen diffusion rate was $7.8 \times 10^{-2} \text{ kg/m}^2\text{-sec}$ which was a factor of four greater than the predicted maximum value at 90 kft in the missile ascent trajectory.

The final phase of this program demonstrated the simultaneous simulation of the critical parameters of an overtest of a 90 kft nuclear encounter. Sustained combustion of the titanium was not observed under any of the test conditions. It is expected that the modeling efforts under Phase II would be able to predict those regions of the parameter space where sustained combustion could occur. If possible, these predictions would be confirmed by simulation experiments.

2-2 COMBUSTION MODEL

The modeling effort began with a brief review of previous studies of titanium combustion/oxidation mechanisms. A kinetic model was then

developed and incorporated into a computer program for parametric analyses.

2-2.1 Titanium Oxidation Kinetics

The characterization of titanium oxidation rate is difficult due to the various oxides which may be present. At least three intermediate oxides (TiO , Ti_2O_3 , TiO_2) may be present in addition to the solid solution of oxygen in titanium. It is also possible that additional oxides (Ti_3O_2 and Ti_3O_3) are formed. With many oxide layers, the rate controlling processes are complex, will change with temperature and pressure, and may be time dependent. As a consequence of the complex activities, the reaction of titanium with oxygen has been the subject of many studies. Earlier work has been reviewed by Hauffe (Reference 1) and Kofstad (Reference 2); the more recent studies have been discussed by Wolf (Reference 3).

At low temperatures a logarithmic rate law has been observed; at higher temperatures (350° to $1,000^{\circ}C$) a parabolic oxidation law has been identified. Experiments at high temperatures (900° to $1,000^{\circ}C$) have also found that a linear oxidation law may dominate which is followed by a decreasing oxidation rate. Besides variations in the oxidation law with temperature, other problems which hamper oxidation modeling are:

- Kinetic constants vary by an order of magnitude between investigators
- All experimental data are from tests longer than 3 min
- All experimental data are from essentially isothermal tests

The most comprehensive model identified in the literature review is by Dunbar, et al. (Reference 4). Reference 4 reviewed previous titanium studies and proposed a model which accounts for both scale buildup over the oxidizing titanium, diffusion of oxygen in-depth (dissolution), and the appropriate energy of reaction (both heat of oxidation and dissolution). For the case of long-term oxygen exposure and isothermal in-depth temperature, this model results in a parabolic rate law that agrees with experimental data. When applied to short-term transient test data, the model was only moderately successful.

The Reference 4 model also does not account for situations in which boundary layer diffusion (rather than subsurface diffusion) dominates the consumption of oxygen. This situation, which may be applicable during a

high altitude atmospheric nuclear encounter, must be considered for a realistic model of the combustion/oxidation phenomenon.

2-2.2 Model Description

The model proposed in this program can be considered to be a modification of the Reference 4 model. One major difference in the present model is the accommodation of a boundary layer, oxygen diffusion-limited reaction case. Similar to the Reference 4 model, the simultaneous formation of an oxide scale (dominated by TiO_2) and the in-bulk dissolution of oxygen are considered. The basic model is exemplified in Figure 1. An oxygen concentration gradient across the scale caused oxygen to diffuse inward. At the TiO_2/Ti interface this oxygen either reacts with Ti to form TiO_2 or continues to diffuse into the Ti region. Both the reaction of oxygen with Ti to form TiO_2 and the dissolution of oxygen into Ti are exothermic processes and result in heat release at the TiO_2/Ti interface.

The model assumes that the concentration gradient is linear and that the diffusion coefficient is approximately constant in the thin TiO_2 region. These assumptions allow the oxygen flux through the scale to be calculated by:

$$\dot{m}_{scale} = \frac{D_1(T_m)}{\xi} (C_a - C_s) \quad (2-1)$$

where

$D_1(T_m)$ = diffusion coefficient of TiO_2 scale at T_m

T_m = mean temperature in TiO_2 scale

ξ = scale thickness

C_a = oxygen concentration at outer surface of scale

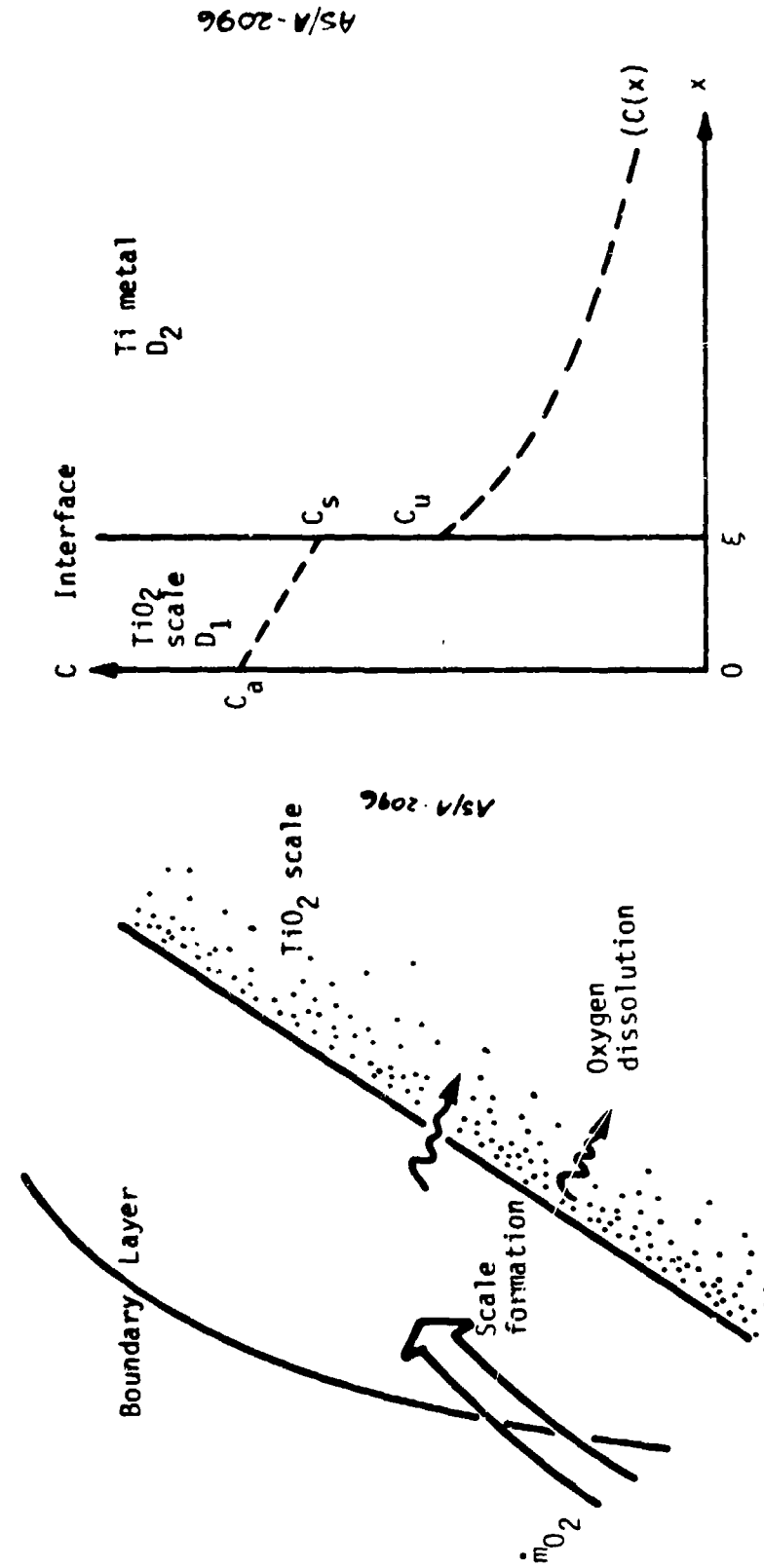
C_s = oxygen concentration at scale-metal interface

In the Ti metal region, the diffusion equation:

$$\frac{\partial C}{\partial t} = \frac{\partial}{\partial x} \left\{ D_2(T) \frac{\partial C}{\partial x} \right\} \quad (2-2)$$

is applied to determine the in-depth oxygen concentration profile. At the TiO_2/Ti interface, one of two boundary conditions is imposed. These boundary conditions are:

Figure 1. Oxidation model and coordinate system.



$$\dot{m}_{\text{scale}} = -D_2(T) \left. \frac{\partial C}{\partial x} \right|_{\xi} \quad (2-3)$$

and

$$C_u = C_{\text{sat}} \quad (2-4)$$

Equation (2-3) is applied when the interface concentration (C_u) is less than the saturation concentration (C_{sat}) (i.e., all oxygen passing through the scale diffuses into the Ti region). C_u , however, is not allowed to rise above the saturation concentration. If the saturation concentration is reached, all oxygen not accommodated by dissolution into the Ti region is forced to react with Ti, adding TiO_2 to the scale layer.

The diffusion coefficients (D_1 and D_2) are modeled by:

$$D_i(T) = A_i \exp\left(-\frac{E_i}{RT}\right) \quad (2-5)$$

Values for A_1 , A_2 , E_1 , and E_2 were calculated by Reference 4 for Ti - 6 Al - 4V. In addition, Reference 4 reports values for C_{sat} , $C_a - C_s$, and the heat of solution (ΔH_{sol}) and oxidation to TiO_2 (ΔH_{ox}). These values are given in Table 1.

Table 1. Combustion model constants for Ti - 6 Al - 4V.

$A_1 = 1,884 \text{ cm}^2/\text{sec}$
$A_2 = 582 \text{ cm}^2/\text{sec}$
$E_1 = 61,800 \text{ cal/mole}$
$E_2 = 61,800 \text{ cal/mole}$
$C_{\text{sat}} = 0.644 \text{ gm/cm}^3$
$C_a - C_s = 0.0144 \text{ gm/cm}^3$
$\Delta H_{\text{ox}} = 12,024 \text{ Btu/lbm}$
$\Delta H_{\text{sol}} = 15,575 \text{ Btu/lbm}$

It should be noted that when the value of $C_a - C_s$ was established in Reference 4, the following assumptions were made: (1) the boundary layer does not limit the oxygen flux to the surface, and (2) $C_a - C_s$ does depend on \dot{m}_{scale} . Ideally, the effect of the boundary layer limitation can be accounted for by solving C_a and C_s independently. This would require a relationship to express C_a as a function of the oxygen partial pressure (p_{O_2}) adjacent to the TiO_2 scale surface. Since such a function is not known, to adjust for boundary layer limitations the mass flux through the scale (\dot{m}_{scale}) was simply not allowed to exceed the value of the oxygen mass flux. Through the boundary layer (\dot{m}_{b1}), which is given by:

$$\dot{m}_{b1} = \rho_e u_e C_m (K_{O_2,e} - K_{O_2,a}) \quad (2-6)$$

where

ρ_e = density of gas at boundary layer edge

u_e = velocity of gas at boundary layer edge

C_m = mass transfer Stanton number

$K_{O_2,e}$ = mass fraction O_2 at boundary layer edge

$K_{O_2,a}$ = mass fraction of O_2 adjacent to TiO_2 scale

A simultaneous solution of Equations (2-1) through (2-6) with a given set of initial and boundary conditions should yield the response of the titanium in accordance with the oxidation model described above. The applicability or usefulness of this model is determined by the degree of agreement between the prediction and actual experimental data. A discussion of this comparison is presented in Section 3.

2-3 COMPUTER CODE OF COMBUSTION MODEL

The transient or time dependent equations of the titanium combustion model were solved numerically. This task was accomplished by modifying the Aerotherm Charring Materials Ablation Code (CMA) to include the titanium combustion model as described in Section 2-2. A detailed description of CMA and its capabilities is not warranted here and the interested reader is referred to Reference 5.

Briefly, CMA is a one-dimensional computer code which calculates the transient thermal and ablation response of a charring material structure. All heat transfer mechanisms -- conduction, convection, and radiation -- are accounted for in CMA. The program can treat complex systems including a main ablating material and several charring and noncharring backup materials. An unusual feature of this code is the capability to handle very general heated surface boundary conditions which may range from simple specified temperature and recession rate to a general thermochemical erosion model incorporating complete chemical erosion computations for any material exposed to a specified environment.

In the present application, modifications were made to CMA to provide an implicit means of calculating in-depth oxygen diffusion phenomena and to account for the appropriate energy release at the TiO_2/Ti boundary according to the model described in the above section. This modified CMA program was the basic tool for prediction and analysis of the e-beam heated titanium combustion data. In addition to the usual input requirements of material properties and boundary conditions, an initial temperature profile of the titanium metal and a heat transfer coefficient are necessary for a typical run. The temperature profile can be calculated from the e-beam energy deposition profile, whereas the heat transfer coefficient is obtained by calibration from surface cooling curves of known flow conditions.

2-4 SIMULATION SYSTEM AND ANALYSIS

A schematic of the simulation experimental configuration is shown in Figure 2. Details of each component were described in the Phase I final report and will not be repeated here. The simulation system consists of an e-beam generator for simulated nuclear irradiation, a variable speed wind tunnel for aerodynamic flows, and a quartz lamp system for controlling titanium bulk temperature.

Simulation parameters of the experimental setup were calibrated for comparison with those of a nuclear encounter. For the most part, the simulated environment was either equivalent or more severe than an actual encounter in terms of catastrophic failure probability. The quartz lamp system (at 2X rated voltage) was able to heat the sample to 1,500K which is higher than the predicted bulk temperatures for the MX shroud monocoque design as shown in Figure 3. Figure 4 shows the predicted oxygen

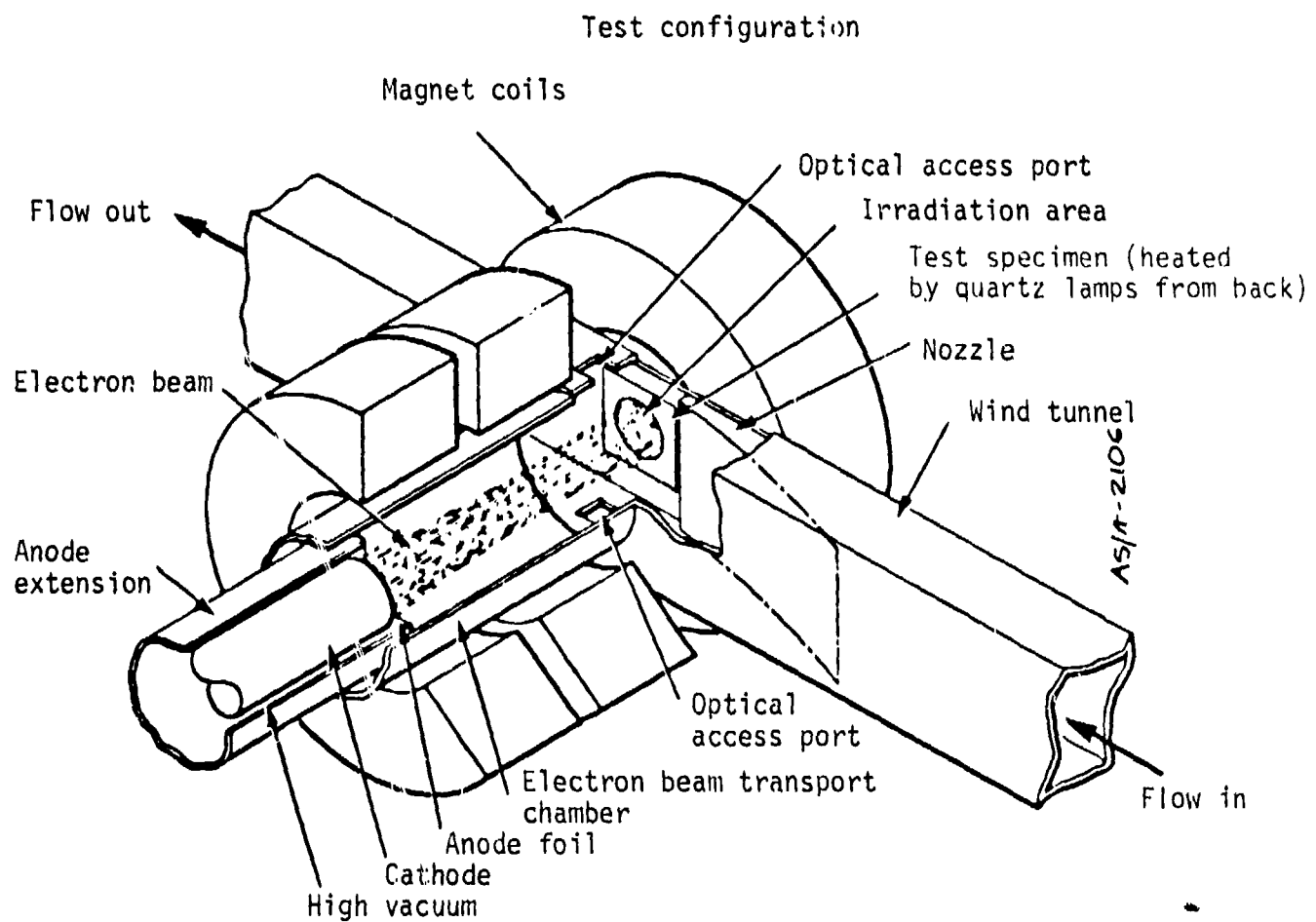


Figure 2. Simulation experimental configuration.

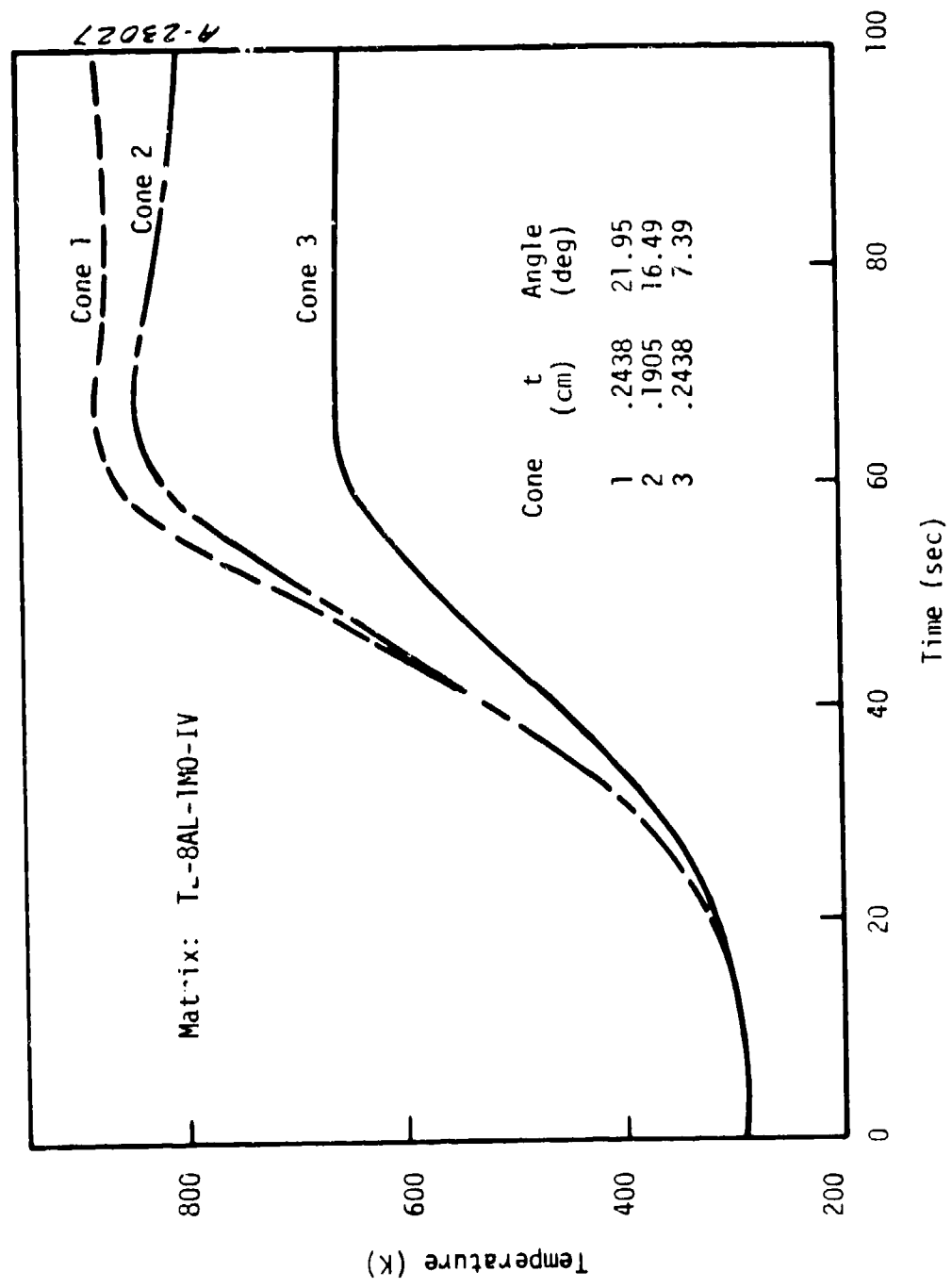


Figure 3. Shroud ascent bulk temperature history.

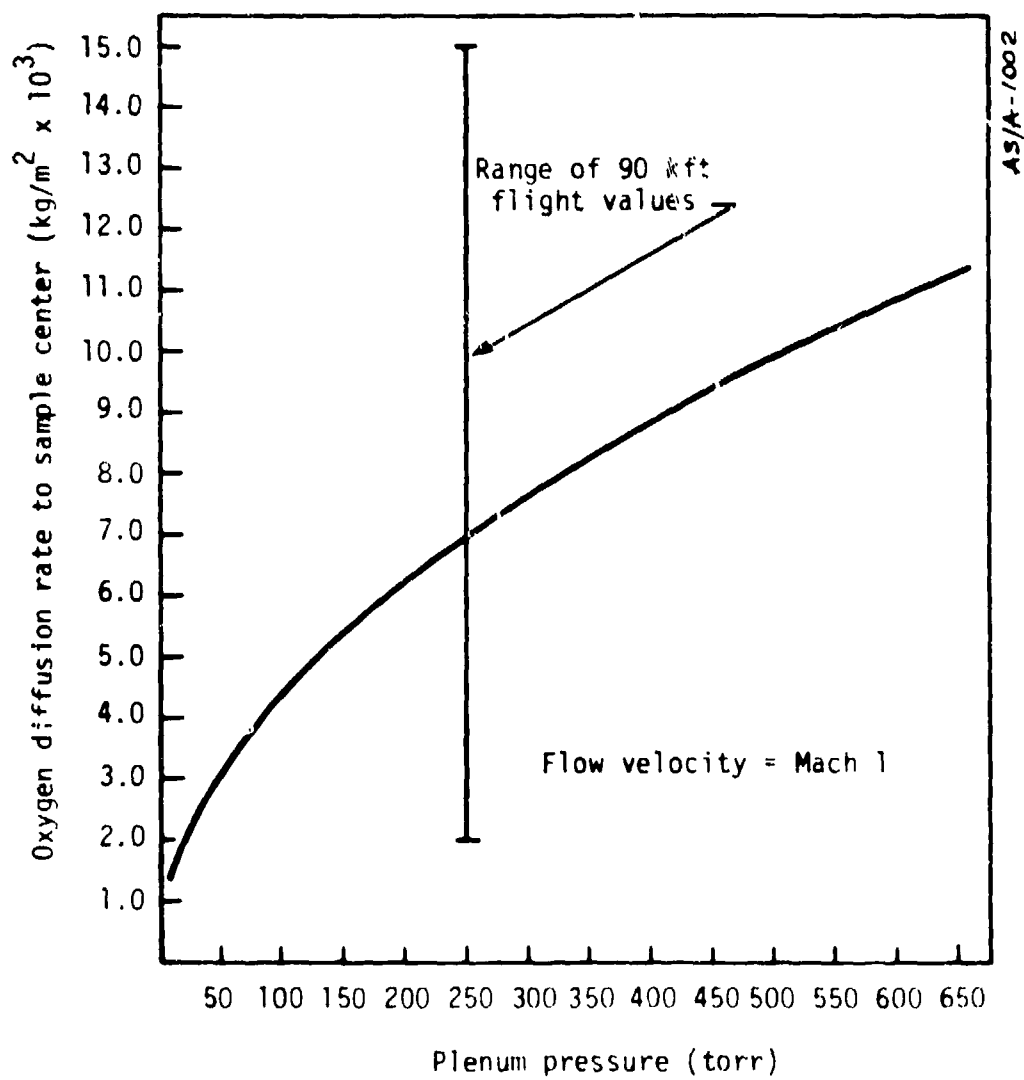


Figure 4. Predicted oxygen diffusion rate to sample surface.

diffusion rate to the sample surface as a function of wind tunnel plenum pressure for a flow velocity of Mach 1 (the wind tunnel was operated in the choked condition for all test runs due to vacuum system design). These predicted values, calculated assuming simple laminar flows over a smooth wall, constitute a lower limit. Actual oxygen diffusion rate for a test run was calculated from the surface temperature cooling curve using heat transfer principles as explained in Section 3. As can be seen from the Figure 4 graph, these calculated oxygen diffusion rates cover the whole range of 90 kft flight values as given in Reference 6 except in the vicinity of the stagnation point.

An analysis was performed to investigate the magnitude of the combustion threat. The analysis was based on an energy balance calculation performed for the time immediately following energy deposition (nuclear or e-beam). When the energy is deposited in the titanium surface, the outermost material is blown off because of the sudden pressure rise and the vaporization of the surface generated by the in-depth deposition. The remaining surface will be at the melt temperature (1,900K for titanium). This process is the same for X-ray or e-beam deposition so the surface temperature is simulated with good fidelity. Since the 1,900K surface temperature is above the 1,600K ignition point for titanium, oxygen diffusing through the boundary layer will cause the surface to combust. The combustion reaction supplies energy to the surface at a rate directly proportional to the oxygen diffusion rate. TiO_x reaction rate kinetics were not included in this analysis since the surface reaction was not kinetically limited and the burning titanium at 1,900K could absorb several orders of magnitude more oxygen than was available.

Energy is transported away from the burning titanium surface by two primary mechanisms: radiation and conduction into the bulk of the material. Radiation loss is dependent on surface temperature and is governed by:

$$Q_{rad} = \epsilon \sigma T^4$$

where Q_{rad} is the radiated energy in W/m^2 , ϵ is the surface emissivity, σ is the Stefan-Boltzmann constant which equals

$5.67 \times 10^{-8} \text{ W/m}^2\text{K}^4$, and T is the surface temperature in K. Conduction into the bulk of the material is governed by the titanium's thermal diffusivity and the surface temperature gradient. To illustrate the conduction loss mechanism, Figure 5 shows a comparison of several X-ray and e-beam deposition profiles. Because the X-ray deposition profiles have a much steeper gradient at the surface than the e-beam profiles, the conduction energy losses from the surface are an order of magnitude larger for X-ray deposition than for the e-beam. Radiative losses are the same for both cases since the surface temperature is the same for either e-beam or X-ray deposition. Convective heat transport losses are so small in comparison to conduction and radiation that they will not be considered here.

Figure 6 illustrates the heat sources and sinks following energy deposition as a function of oxygen availability, surface temperature, and surface temperature gradient. If the TiO_x reaction energy exceeds the sum of the conductive and radiative losses, the surface temperature will be rising and sustained combustion is probable. If the losses are greater than the reaction energy, the surface temperature will decrease and the combustion process will cease.

Table 2 lists the analysis parameters for both the nuclear encounter and the e-beam simulation experiment under Phase I. Using the energy balance model described above, it is obvious that sustained combustion is unlikely for either case. The prediction was confirmed by actual Phase I experimental results which showed no sample combustion failure under all test conditions, which included a good overtest of the nuclear encounter case. Phase II experimental efforts encompass an attempt to induce sustained combustion of titanium using the simulation system and, if achieved, explain such behavior by the combustion model. Results of these efforts are presented in the following section.

AS/A - 2/05

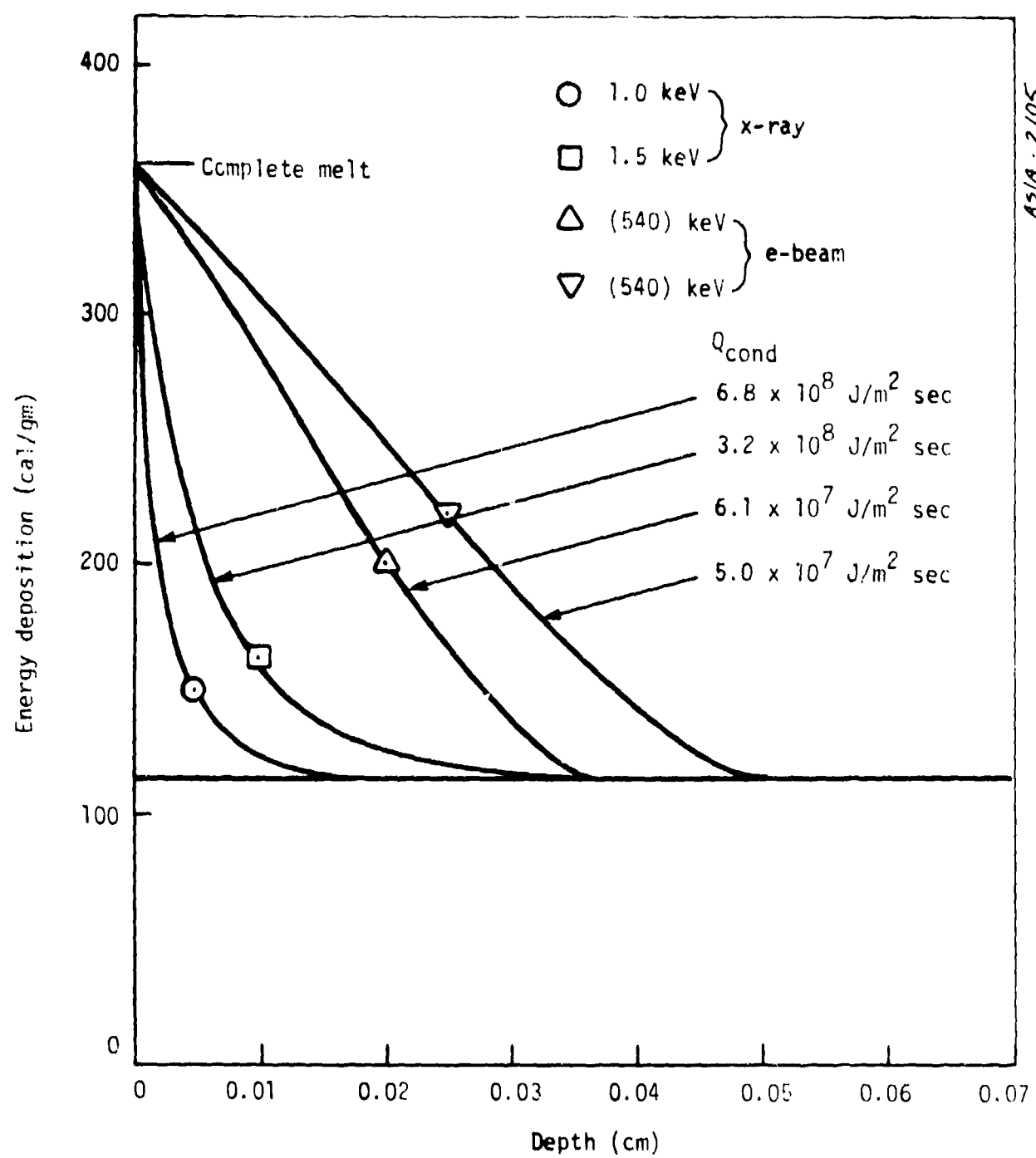
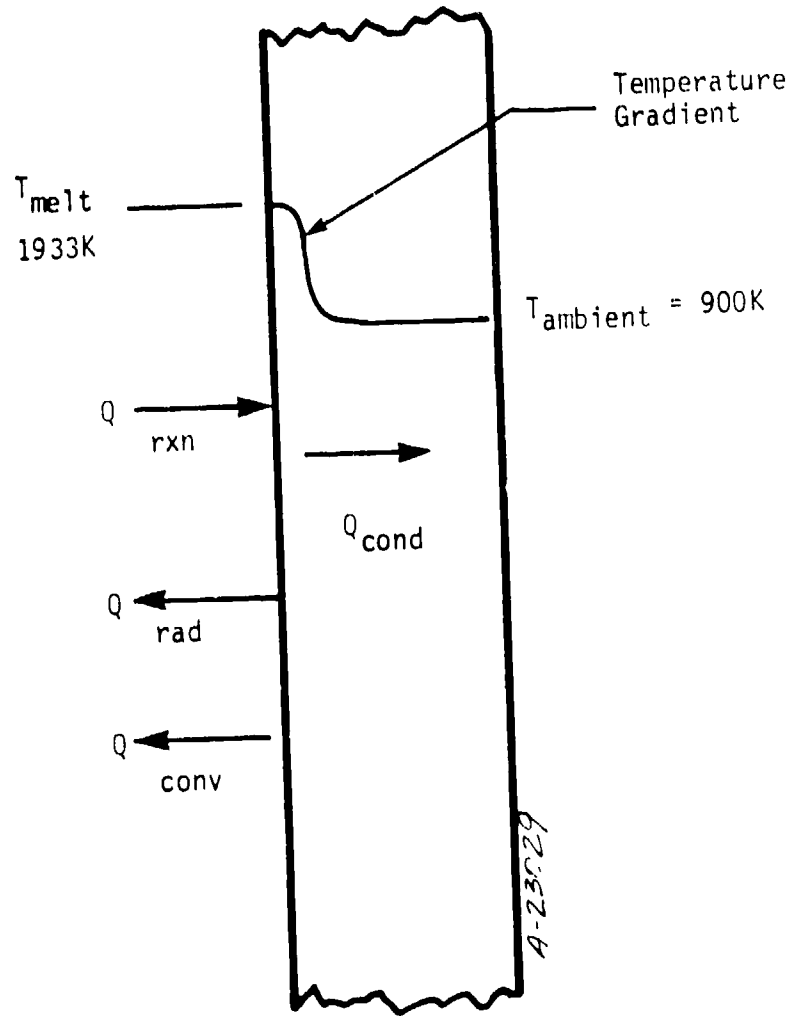


Figure 5. Comparison of e-beam and X-ray deposition profiles.



$$Q_{rxn} \doteq Q_{cond} + Q_{conv} + Q_{rad}$$

Figure 6. Energy requirements for combustion.

Table 2. Nuclear environment versus simulation parameters.

	Nuclear Threat	E-Beam Simulation
Bulk temperature	900K	900K
Surface temperature	1,900K	1,900K
Q_2 diffusion	$\leq 4.80 \times 10^{-2} \text{ kg/m}^2 \text{ sec}$	$7.8 \times 10^{-2} \text{ kg/m}^2 \text{ sec}$
$Q_{\text{conduction}}$	$3.2 - 6.8 \times 10^8 \text{ J/m}^2 \text{ sec}$	$5.0 - 6.1 \times 10^7 \text{ J/m}^2 \text{ sec}$
$Q_{\text{radiation}}$	$4.0 \times 10^5 \text{ J/m}^2 \text{ sec}$	$4.0 \times 10^5 \text{ J/m}^2 \text{ sec}$
Q_{reaction}	$\leq 1.4 \times 10^6 \text{ J/m}^2 \text{ sec}$	$2.2 \times 10^6 \text{ J/m}^2 \text{ sec}$

SECTION 3

RESULTS AND CONCLUSIONS

3-1 TEST MATRIX AND DATA SUMMARY

Operation and calibration of the experimental facility were described in the Phase I report and will not be repeated here except for modifications. Table 3 shows a summary of the test matrix under the Phase II efforts. The rationale for this matrix is as follows: the simulation system is to be operated under the most severe conditions in an attempt to cause sustained combustion of the titanium, and if successful the parameters will be modified to define minimum conditions for sustained combustion.

Wind tunnel performance was monitored with a static pressure transducer located on the tunnel wall downstream from the trailing edge of the sample. Since the wind tunnel is operated in the choked flow mode, this single pressure was sufficient to record the tunnel performance (a constant ratio of 0.528 always exists between the static and upstream plenum pressures). Titanium surface temperature was recorded by a fast response optical pyrometer which had been previously calibrated for titanium using the quartz lamps as heat source and chromel-alumel thermocouple as reference. Pressure and temperature data were recorded on oscilloscopes. Preliminary e-beam shots were used to characterize the beam in terms of electron energy spectrum, fluence, and uniformity. Fluence for each test was calculated from measured e-beam voltage and current and was provided by PI.

The oxygen diffusion rate to the sample surface was estimated from cooling curves of the sample surface under various operating conditions. The technique is based on heat transfer principles and involves simplifying assumptions. A typical experimental procedure for such a

Table 3. Data summary of test matrix.

Test Number	Sample Material	Sample Thickness (mm)	Preheat Temperature (K)	Fluence (cal/cm ²)	Oxygen Diffusion Rate (kg/m ² -sec)	Postdeposition Bulk Temperature (K)	Average Crater Depth (mm)	Comments
NAA	Ti alloy	1.55	1,700	NA	0.17	NA	NA	No e-beam
2267	Ti alloy	1.55	1,545	43	0.17	NA	NA	Burnthrough with notch
2268	Ti alloy	1.55	1,530	NA	0.17	NA	NA	Burnthrough with notch
2270	Ti alloy	1.53	1,525	42	0.057	NA	NA	Burnthrough
2271	Ti alloy	2.07	1,375	19	0.057	1,477	0.033	Poor e-beam output; surface etched
2272	Ti alloy	2.07	1,325	45	0.057	1,465	0.351	No burnthrough; surface etched
2273	Ti alloy	2.04	1,318	30	0.057	1,430	0.147	Poor e-beam output; surface etched
2274	Ti alloy	2.08	1,303	20	0.057	1,400	NA	Poor e-beam output; surface etched
2278	Ti alloy	2.05	1,242	53	0.057	1,410	0.421	No burnthrough; melt streak
2279	Inconel 600	1.88	1,235	52	0.057	1,311	0.189	No burnthrough; melt streak
2280	Inconel 600	1.88	1,350	53	0.057	1,394	0.126	No burnthrough

aNA -- not applicable/available

calibration is as follows: the sample is heated to a steady-state temperature by the quartz lamps with no flow; the wind tunnel is turned on and the surface temperature history is recorded.

Under steady-state conditions with no flow, the lamp heat flux absorbed by the sample would equal the radiation and conduction losses (natural convection loss is relatively small and is not considered here). With the airflow on, steady-state conditions no longer exist and the surface temperature will decrease due to convective cooling. For a thin sample, i.e., assuming no temperature gradient existed in the material, the convective heat transfer coefficient, \bar{h} , can be calculated from the following equation:

$$\dot{q}_{\text{loss}} = \dot{q}_{\text{conv}}$$

or

$$t\rho c_p \frac{dT}{d\theta} = \bar{h}(T - T_\infty) \quad (3-1)$$

where

$$\frac{dT}{d\theta} = \text{surface cooling rate}$$

t , ρ , c_p = sample thickness, density and specific heat, respectively

T_∞ = ambient temperature

Assuming that the Stanton numbers for heat and mass transfers are equal and recalling Equation (2-6), the oxygen diffusion rate onto the sample surface is given by:

$$\begin{aligned} \dot{m}_{b1} &= \rho_e u_e c_m (K_{O_2,e} - K_{O_2,a}) \\ &= \frac{\bar{h}}{c_p} (K_{O_2,e} - K_{O_2,a}) \end{aligned} \quad (3-2)$$

For air, assuming all oxygen at the titanium surface has either reacted or been absorbed, i.e., $K_{O_2,a} = 0$, then:

$$\dot{m}_{b1} = 0.232 \frac{\bar{h}}{c_p} \quad (3-3)$$

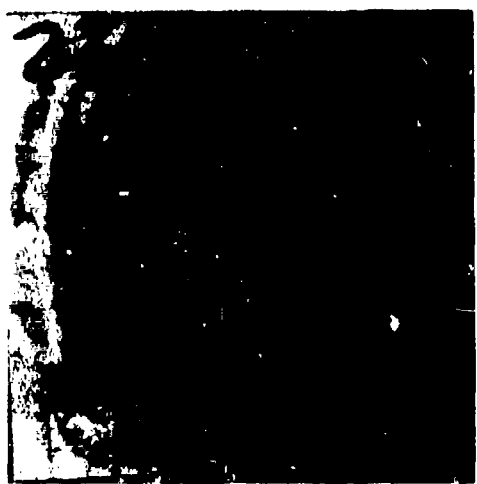
The oxygen diffusion rate values listed in Table 3 represent an average of several calibration runs for each of the two flow conditions. These values were also used in the modeling efforts.

The first run in the test matrix was carried out to observe whether spontaneous combustion would occur for a sample bulk temperature in excess of the published ignition point of 1,600K. The temperature decreased steadily as the flow was turned on and no combustion was observed as expected. Even though the bulk temperature was higher than ignition, very little oxygen was available at the Ti/TiO₂ interface due to oxide scale buildup. No scale removal mechanism was provided as in the case for a nuclear or e-beam encounter.

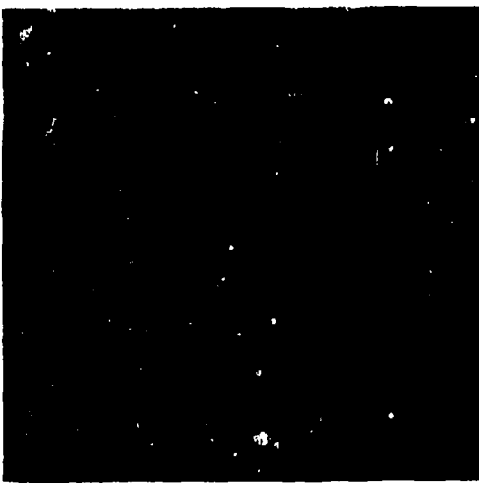
Tests 2267 and 2268 were run under almost identical conditions: maximum oxygen diffusion to the surface, preheat temperatures of about 1,540K, and a fluence of 43 cal/cm² (no data for fluence was available for Test 2268 but the e-beam was operated under the same conditions as Test 2267). Samples in both tests failed with complete burnthrough over the irradiated areas. Postrun photos of selected tested samples are shown in Figure 7. Temperature and pressure traces for Test 2268 are shown in Figure 8 in comparison with those for Test 2272 where no sample failure occurred. Sudden noise observed on the signal traces for Test 2268 was a typical indication of an impending sample failure.

Test 2270 was conducted under conditions similar to the previous two runs except with reduced flow (approximately one-third in oxygen diffusion rate). The sample failed as in the previous tests.

For Test 2271, the sample bulk temperature was decreased by 150 to 1,375K, while other operating conditions were held constant. Also, the sample thickness was increased from 1.55 mm to 2.02 mm due to an exhausted supply of the thinner samples. The e-beam malfunctioned producing a donut-shaped beam with a low fluence. No burnthrough of the sample occurred; a ring-shaped pattern was etched on the sample surface as shown in Figure 7.



TEST 2268



TEST 2270



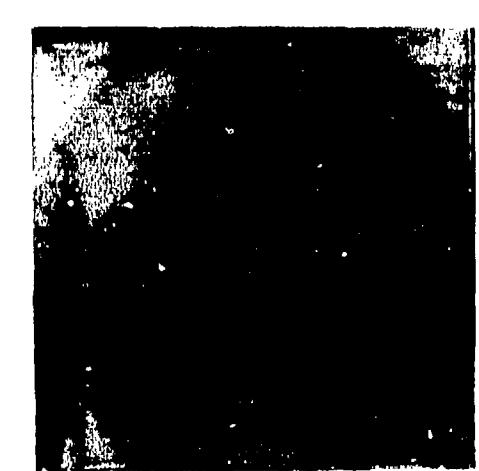
TEST 2271



TEST 2272



TEST 2278



TEST 2279

AS H-1048D

Figure 7. Postrun photos of tested samples.

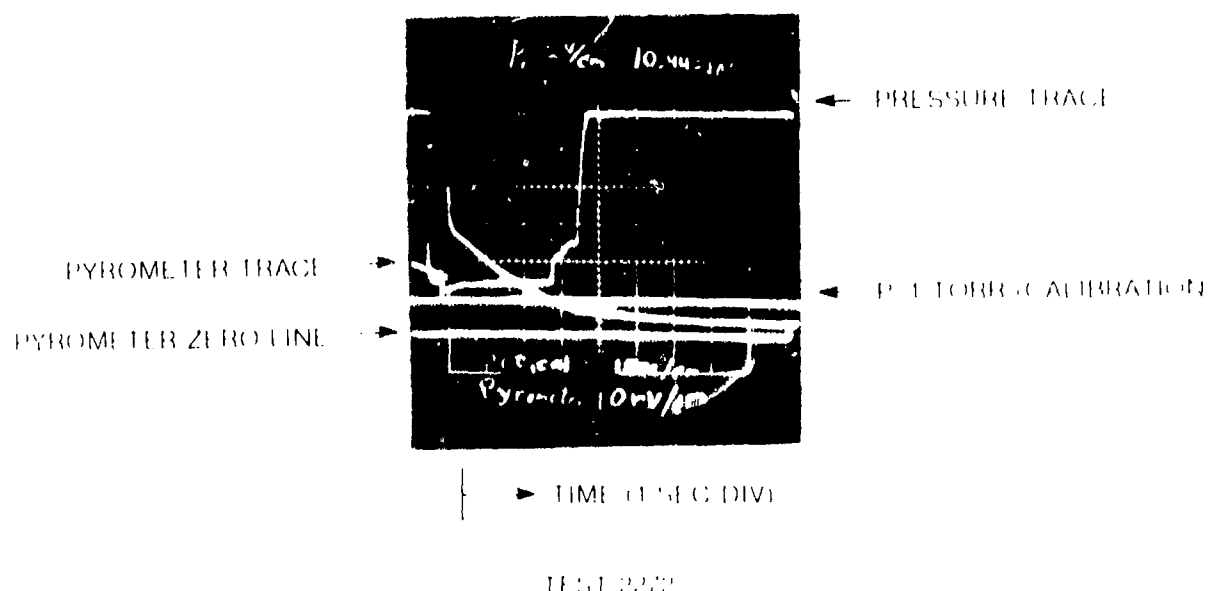
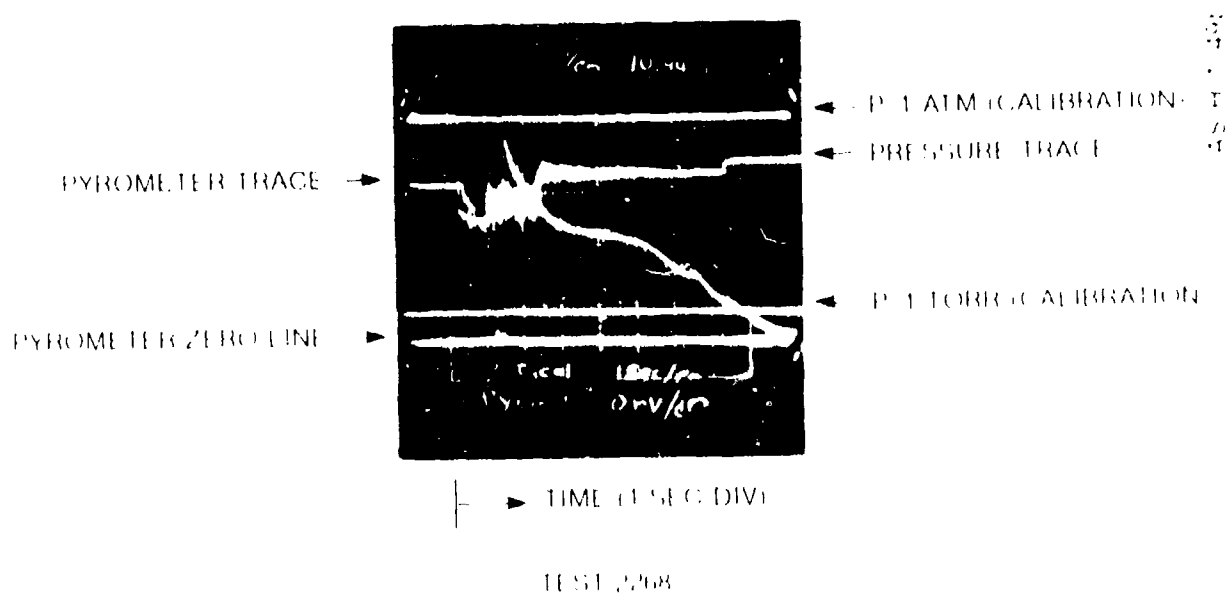


Figure 8. Oscilloscope traces for Tests 2268 and 2272.

Everything functioned as planned for Test 2272. No sustained combustion or catastrophic failure of the sample was observed with reduced bulk temperature in contrast to Test 2270; the sample was etched uniformly over the irradiated area.

Tests 2273 and 2274 were unsuccessful attempts to duplicate Test 2272; the e-beam performance was erratic. No sample failures occurred as would be expected under the reduced fluence conditions.

Efforts to stabilize the e-beam output were undertaken prior to Test 2278. Again, no sustained combustion of the sample was noted under somewhat reduced bulk temperature (the quartz lamps were deteriorating) and higher fluence conditions. Postrun surface conditions were similar for Tests 2271 through 2278 except for crater depth, probably indicating no change in burn or wear mechanisms.

Inconel-600 samples were used in Tests 2279 and 2280 at bulk temperatures of 1,235 and 1,350K. No sample burnthrough was observed in either test under relatively high fluence of 52 cal/cm². The Inconel samples were tested primarily to observe their behavior under simulated nuclear encounter environment. No analysis or prediction of response was performed under the present work scope.

A complete mapping of the parameters for sustained titanium combustion was not undertaken as part of the test matrix for this project. The matrix demonstrated that sustained combustion could occur under certain conditions. The test matrix also demonstrated that the sample preheat temperature is an important parameter in inducing sample failure under the tested flows and fluence conditions. The two tested flowrates indicate that failure will occur if the bulk temperature is high enough to cause the e-beam fluence to raise the postdeposition bulk temperature above the titanium ignition temperature of 1,600K.

3-2 COMPARISON OF ANALYTIC AND EXPERIMENTAL RESULTS

Analytical efforts concentrated on predicting the experimental results of the two distinct cases of either sample failure or survival. Test 2268 typifies the case of sample burnthrough, whereas Test 2272 represents sample survival. Sample temperature is the key criterion for sample behavior in the computer model. After e-beam deposition and the accompanying surface layer burnoff and/or meltdown, the bulk temperature will either increase or decrease, depending on the energy balance between

chemical heat generation and radiative and convective losses. A sustained temperature increase toward the melting point indicates sample failure, whereas a gradual decay is expected for sample survival. While no surface temperature data were available for cases of burnthrough, good surface temperature data existed for the nonburn cases enabling the analytical predictions to be checked for reliability and usefulness.

In addition to the usual material properties and flow specifications, input requirements for a modified CMA run include a postdeposition sample temperature profile. This temperature profile was calculated using the e-beam absorption profile supplied by PI for each test and the specific heat curve of titanium. Due to the variations of e-beam energy, there were slight dissimilarities. Consequently, the temperature profile was computed separately for each test.

Computer runs of Tests 2268 and 2272 were conducted. Initial results showed that while the response of Test 2272 was predicted quite satisfactorily, no sample failure was noted for Test 2268. In fact, no sustained temperature rise of the sample was predicted for all cases of the test matrix. Reexamination of the combustion model as incorporated in CMA revealed no significant errors except that CMA does not provide for scale or oxide removal once it is formed on the surface. The gradual scale buildup in this case formed an oxygen diffusion barrier that essentially quenched any further heat producing oxidation.

This scale buildup in the model is in contrast to the experimental observation of the posttest samples which showed little evidence of a permanent scale layer even in cases of very low e-beam energy. A scale thickness limitation was incorporated into the combustion model, and the two test cases were rerun with various arbitrary scale thicknesses.

Analysis of the computer output showed that with a scale thickness limit of 5.08×10^{-5} cm (2.0×10^{-5} in.), model predictions agreed very well with the experimental results. Figure 9 shows the postdeposition temperature history of Test 2272. The agreement between the prediction and experimental values is excellent, indicating that the temperature decays steadily with no sustained combustion. The scale thickness limitation had little effect on the predicted temperature; maximum scale thickness was barely above the limit in this case. The value of 5.08×10^{-5} cm was chosen as one of the scale thickness limits

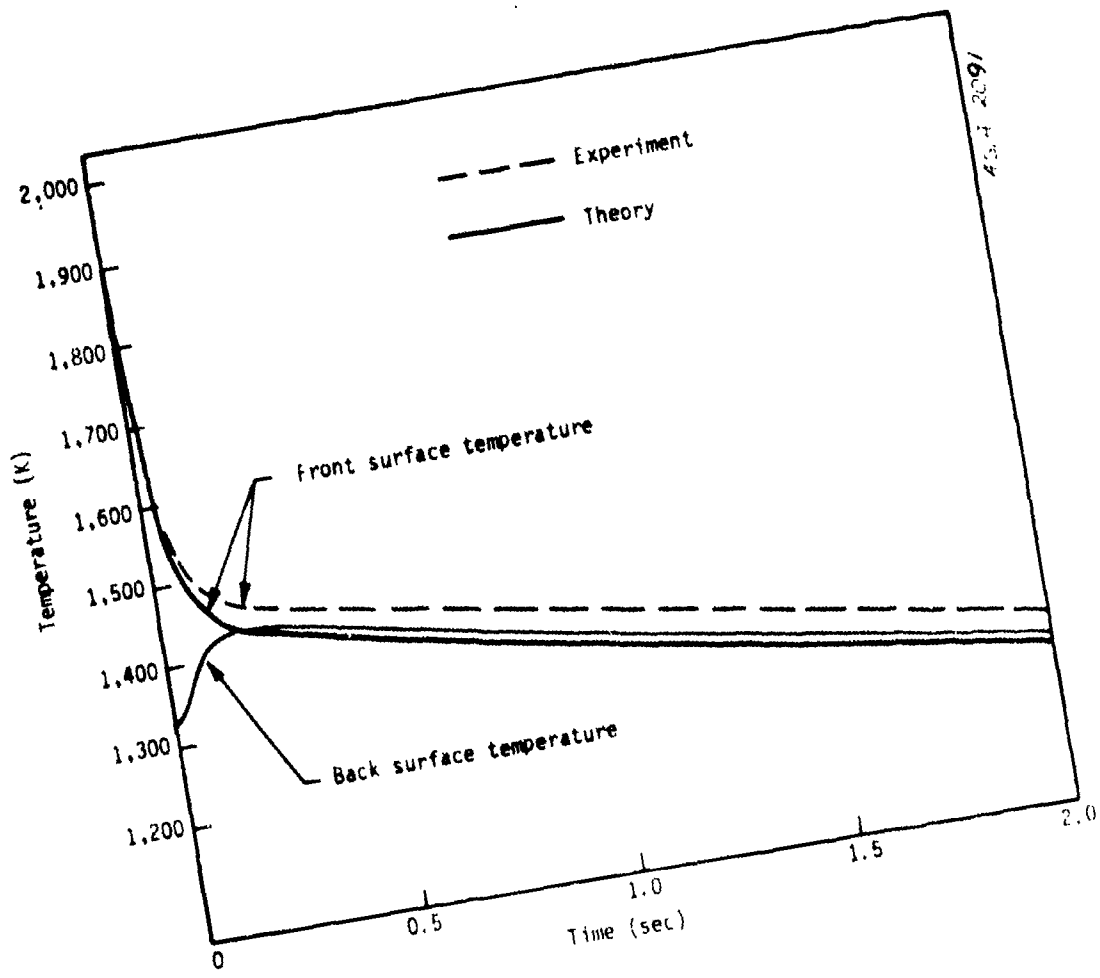


Figure 9. Postdeposition temperature history of Test 2272.

for investigation to avoid significantly altering the model prediction for this case which compared favorably with experimental measurement in the initial computer runs.

Figure 10 shows the predicted temperature history for Test 2268. After an initial decline, the front surface temperature rises to the titanium melting temperature in approximately 300 ms at which point catastrophic failure of the sample begins. This is again in excellent agreement with the experimental result which shows that the pressure fluctuates approximately 0.3 sec after the e-beam deposition as shown in Figure 8. The sample temperature was not calculated beyond 300 ms since the combustion model is not applicable when the surface begins to melt.

Finally, the combustion model was utilized to analyze the surface temperature response under a nuclear encounter at 90 kft. As expected, no sample failure occurs and the sample essentially remains at the preencounter bulk temperature after an initial surge near the front surface. Figure 11 shows the results of such an encounter.

3-3 CONCLUSIONS AND RECOMMENDATIONS

This program has achieved its objective: to develop a methodology for predicting the response of the titanium surface and confirm the accuracy of the model through an analysis of the experimental data. The combustion model considers all pertinent reaction phenomena and utilizes the most up-to-date material constants. It was then fully incorporated into an existing computer program and case studies were made that corresponded to experimental conditions. Excellent agreement between the model prediction and experimental result was obtained. Model analysis of a 90 kft nuclear encounter showed that such environmental conditions would not cause a failure of the titanium shroud.

The experimental simulation system was able to demonstrate conditions under which the titanium sample failed catastrophically. These conditions, however, are not expected to exist for the present advanced missile system launch trajectories. No sample failure was observed under simulated environment for a 90 kft nuclear encounter. The test matrix did not fully map out environmental conditions under which sample failure may occur.

Based on the apparent success of the combustion model in predicting the experimental results, a full-scale parametric study of the titanium

AS14-2092

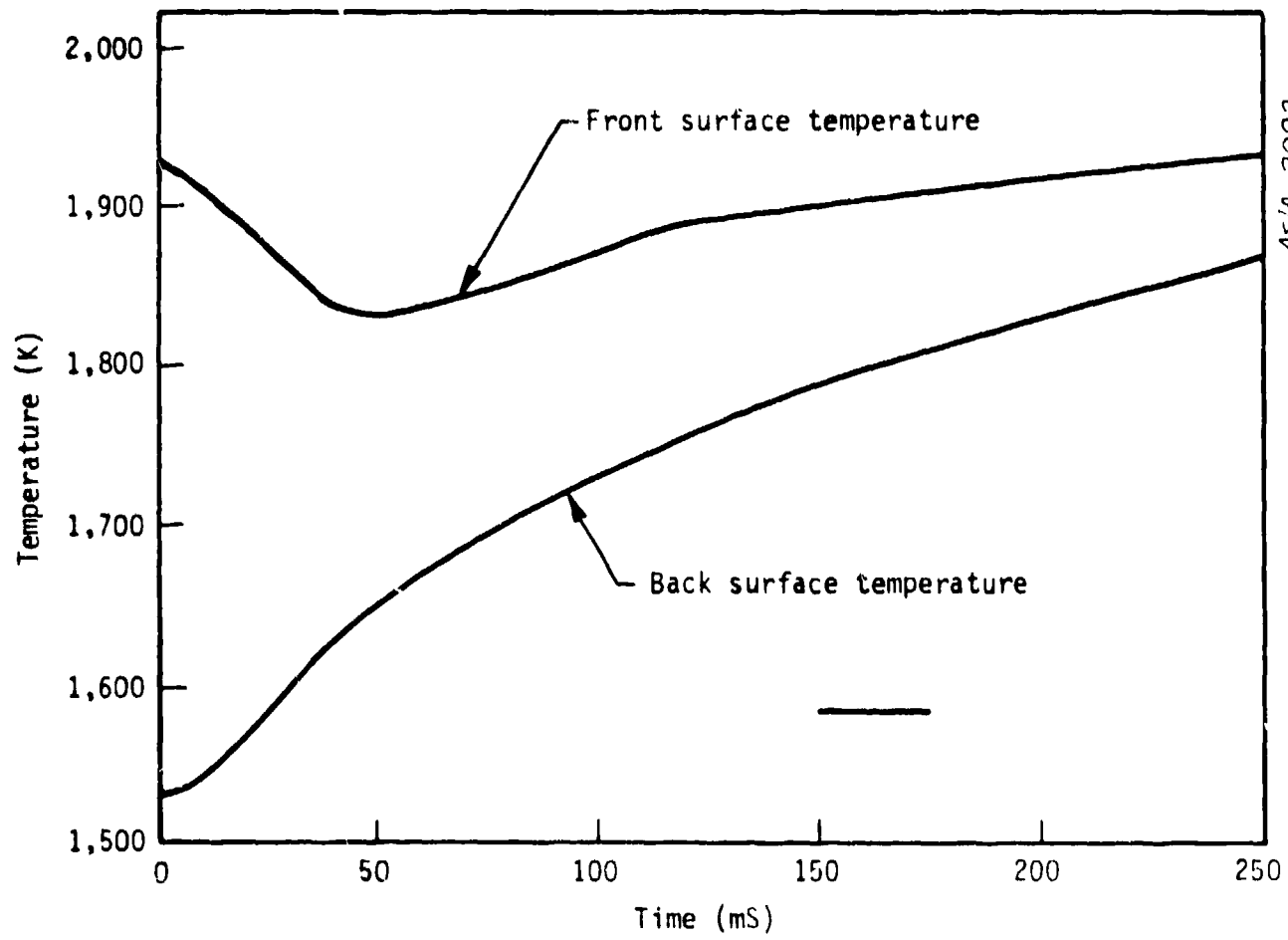


Figure 10. Predicted temperature history of Test 2268.

AS/A-2093

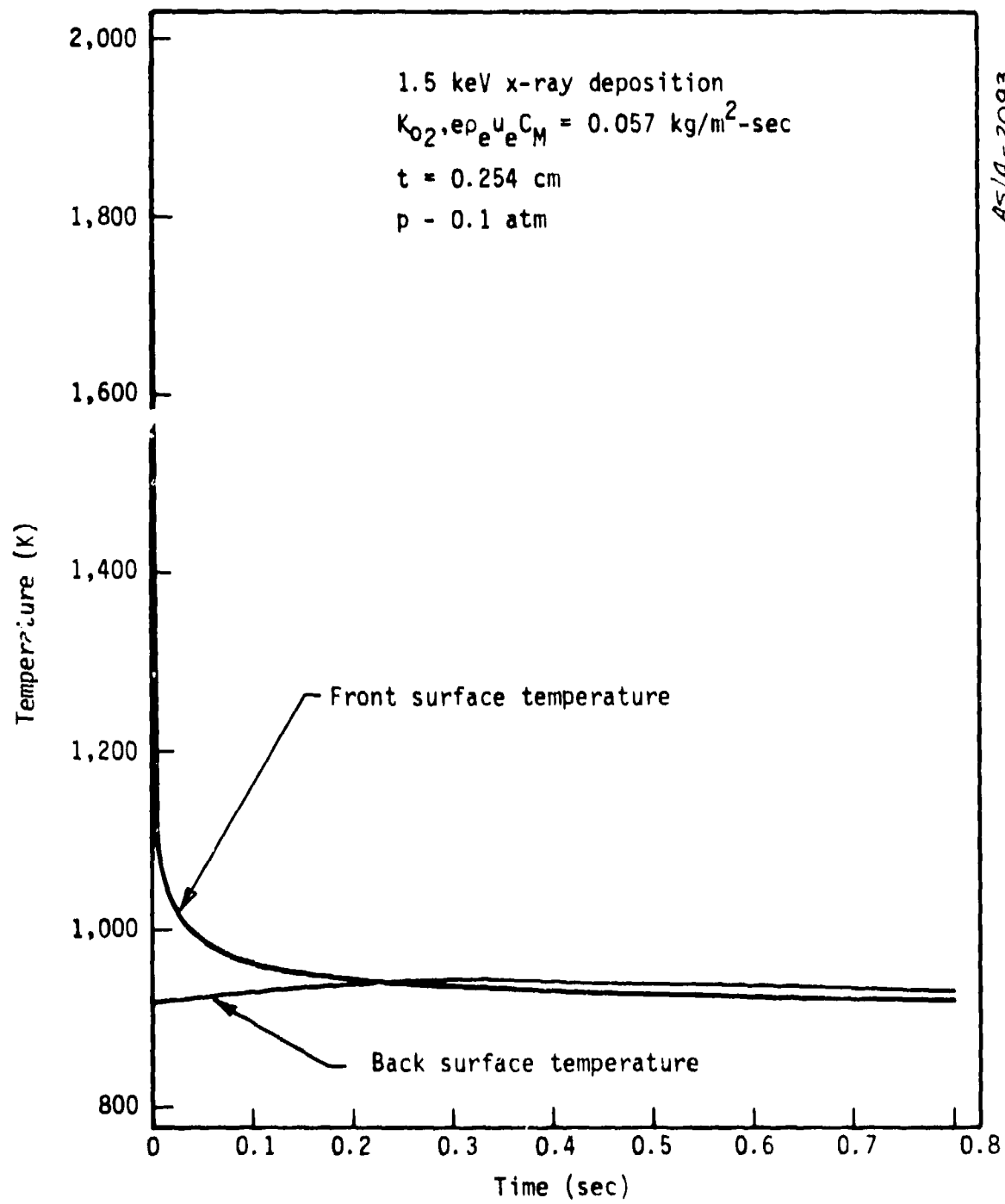


Figure 11. Predicted temperature history of a 90 kft nuclear encounter.

oxidation is recommended. An experimental test matrix should be performed for verification of the model predictions. The ultimate goal is to develop a high confidence model in which titanium response under any given conditions can be predicted.

SECTION 4
REFERENCES

1. Hauffe, K., Oxidation of Metals, Plenum, New York, 1965.
2. Kofstad, P., High Temperature Oxidation of Metals, Wiley, New York, 1966.
3. Wolf, J. S., "Exploratory Development on Oxidation Behavior of Titanium Alloys Under High Heating Rates," Technical Report, AFML TR-74-265, April 1975.
4. Dunbar, L. E., et al., "Titanium Response in Oxidizing Environments," presented at 2nd AIAA/ASME Thermophysics and Heat Transfer Conference, Palo Alto, California, May 24-26, 1978.
5. "Aerotherm Charring Material Thermal Response and Ablation Program," Aerotherm Report No. UM-70-14, April 1970.
6. Maegley, W. J., "MX Aerodynamic Heating Data," Report No. SE-0016, Martin Marietta Corporation, December 1978.

DISTRIBUTION LIST

DEPARTMENT OF DEFENSE

Assistant to the Secretary of Defense
 Atomic Energy
 ATTN: Executive Assistant

Defense Communications Agency
 ATTN: CCTC

Defense Intelligence Agency
 ATTN: DT-2, T. Dorr
 ATTN: DT-2
 ATTN: DT-1C
 ATTN: DB-4D

Defense Nuclear Agency
 ATTN: NATA
 ATTN: STNA
 ATTN: SPSS
 ATTN: SPTD
 ATTN: STSP
 3 cy ATTN: SPAS
 4 cy ATTN: TITL

Defense Technical Information Center
 12 cy ATTN: DD

Field Command
 Defense Nuclear Agency
 ATTN: FCTMOF
 ATTN: FCPR
 ATTN: FCTOF
 ATTN: G. Ganong

Field Command
 Defense Nuclear Agency
 Livermore Branch
 ATTN: FCPR

Joint Chiefs of Staff
 ATTN: SAGA/SSD
 ATTN: J-5, Nuclear Division
 ATTN: J-5, Force Planning & Program Div
 ATTN: SAGA/SFD

Joint Strat Tgt Planning Staff
 ATTN: JLW-2
 ATTN: JLA
 ATTN: JPST, G. Burton
 ATTN: JPST
 ATTN: JPTM

NATO School (SHAPE)
 ATTN: U.S. Documents Officer

Under Secy of Def for Rsch & Engrg
 Department of Defense
 ATTN: Engr Technology, J. Persh
 ATTN: Strat & Space Sys (OS)

DEPARTMENT OF THE ARMY

BMD Advanced Technology Center
 Department of the Army
 ATTN: ATC-T, M. Capps

DEPARTMENT OF THE ARMY (Continued)

BMD Systems Command
 Department of the Army
 ATTN: BMDSC-H, N. Hurst

Dep Ch of Staff for Ops & Plans
 Department of the Army
 ATTN: DAMO-NCZ

Dep Ch of Staff for Rsch Dev & Acq
 Department of the Army
 ATTN: DAMO-CSS-N

Harry Diamond Laboratories
 Department of the Army
 ATTN: DELHD-N-TF
 ATTN: DELHD-N-P, J. Gwaltney
 ATTN: DELHD-N-P

U.S. Army Ballistic Research Labs
 ATTN: DRDAR-BLV
 ATTN: DRDAR-BLT, J. Frasier
 ATTN: DRDAR-BLV, W. Schuman, Jr.
 ATTN: DRDAR-BLT, J. Keefer
 ATTN: DRDAR-BLT, R. Vitali
 ATTN: DRDAR-BL, R. Eichelberger

U.S. Army Material & Mechanics Rsch Ctr
 ATTN: DRXMR-HH, J. Dignam

U.S. Army Materiel Dev & Readiness Cmd
 ATTN: DRCDE-D, L. Flynn

U.S. Army Missile Command
 ATTN: DRSMI-RHB, H. Greene
 ATTN: DRSMI-RKP, W. Thomas
 ATTN: DRSMI-XS

U.S. Army Nuclear & Chemical Agency
 ATTN: Library

U.S. Army Research Office
 ATTN: P. Radowski Consultant

U.S. Army TRADOC Sys Analysis Actvty
 ATTN: ATAA-TDC, R. Benson

DEPARTMENT OF THE NAVY

Naval Research Laboratory
 ATTN: Code 4773, G. Cooperstein
 ATTN: Code 2627
 ATTN: Code 7908, A. Williams

Naval Sea Systems Command
 ATTN: SEA-0352, M. Kinna

Naval Surface Weapons Center
 ATTN: Code R15, J. Petes
 ATTN: Code K06, C. Lyons
 ATTN: Code F31

Naval Weapons Evaluation Facility
 ATTN: Code 70, L. Oliver
 ATTN: P. Hughes

DEPARTMENT OF THE NAVY (Continued)

Office of Naval Research
ATTN: Code 465

Office of the Chief of Naval Operations
ATTN: OP 654E14, R. Blaise
ATTN: OP 654C3, R. Piacesi
ATTN: OP 65

Strategic Systems Project Office
Department of the Navy
ATTN: NSP-273
ATTN: NSP-272
ATTN: NSP-2722, F. Wimberly

DEPARTMENT OF THE AIR FORCE

Aeronautical Systems Division
Air Force Systems Command
2 cy ATTN: ASD/ENFTV, D. Ward

Air Force Aeronautical Lab
Materials Laboratory
ATTN: LLM, T. Nicholas
ATTN: MBC, D. Schmidt

Air Force Geophysics Laboratory
ATTN: LY, C. Touart

Air Force Rocket Propulsion Lab
ATTN: LKCP, G. Beale

Air Force Systems Command
ATTN: XRTD
ATTN: SOSS

Air Force Technical Applications Ctr
ATTN: TF

Air Force Weapons Laboratory, AFSC
ATTN: NTES, K. Filippelli
ATTN: NTYV, A. Sharp
ATTN: DYV
ATTN: SUL
ATTN: HO, W. Minge
ATTN: DYV, E. Copus
2 cy ATTN: NTO

Air Force Wright Aeronautical Lab
Flight Dynamics Laboratory
ATTN: FXG
ATTN: FBAC, D. Roselius

Air Force Wright Aeronautical Lab
ATTN: MLB, G. Schmitt

Air University Library
Department of the Air Force
ATTN: AUL-LSE

Arnold Engng Dev Ctr, AFSC
Department of the Air Force
ATTN: AEDC, AFSC/DOOP, G. Cowley
ATTN: AEDC, AFSC/Library Documents

Ballistic Missile Office
Air Force Systems Command
ATTN: MNMR
ATTN: MNRTE
ATTN: MNN
2 cy ATTN: MNNXH, Blankinship
3 cy ATTN: MNNXH, J. Allen

DEPARTMENT OF THE AIR FORCE (Continued)

Deputy Chief of Staff
Operations Plans and Readiness
Department of the Air Force
ATTN: AFXO OSS

Deputy Chief of Staff
Research, Development & Acq
Department of the Air Force
ATTN: AFROQI
ATTN: AFRD

Foreign Technology Division
Air Force Systems Command
ATTN: SDBG
ATTN: TQTD
ATTN: SDBS, J. Pumphrey

Headquarters Space Division
Air Force Systems Command
ATTN: RST
ATTN: RSS

Headquarters Space Division
Air Force Systems Command
ATTN: AFML, G. Kirshner

Strategic Air Command
Department of the Air Force
ATTN: XORM
ATTN: DOXT
ATTN: XPPS
ATTN: XPM

DEPARTMENT OF ENERGY

Department of Energy
ATTN: OMA/RD&T

OTHER GOVERNMENT AGENCY

Central Intelligence Agency
ATTN: OSWR/NED

DEPARTMENT OF ENERGY CONTRACTORS

Lawrence Livermore National Laboratory
ATTN: L-125, J. Keller
ATTN: L-24, G. Stahle
ATTN: L-262, J. Knox
ATTN: L-92, C. Taylor

Los Alamos National Scientific Laboratory
ATTN: MS 670, J. Hopkins
ATTN: J. Taylor
ATTN: R. Dingus
ATTN: D. Kerr
ATTN: J. McQueen
ATTN: R. Thurston

Sandia National Laboratories
ATTN: A. Chabria
ATTN: M. Cowan

Sandia National Laboratories
Livermore Laboratory
ATTN: H. Norris
ATTN: T. Cook
ATTN: Library & Security Class Div

DEPARTMENT OF DEFENSE CONTRACTORS

Aurex Corp
 ATTN: R. Rindal
 ATTN: C. Nardo
 ATTN: C. Powers
4 cy ATTN: K. Triebes
4 cy ATTN: G. Liu

Aerojet Solid Propulsion Co
 ATTN: R. Steele

Aeronautical Rsch Assoc of Princeton, Inc
 ATTN: C. Donaldson

Aerospace Corp
 ATTN: R. Crolius
 ATTN: J. McClelland
 ATTN: H. Biaes
 ATTN: W. Barry

Analytic Services, Inc
 ATTN: J. Selig

Aptek, Inc
 ATTN: T. Meagher

Avco Research & Systems Group
 ATTN: W. Reinecke
 ATTN: P. Grady
 ATTN: Document Control
 ATTN: W. Broding
 ATTN: J. Gilmore
 ATTN: J. Stevens
 ATTN: A. Pallone

Battelle Memorial Institute
 ATTN: E. Unger
 ATTN: M. Vanderlind
 ATTN: R. Castle

Boeing Co
 ATTN: M/S 85/20, E. York
 ATTN: R. Dyrdahl
 ATTN: B. Lempiere
 ATTN: R. Holmes

California Research & Technology, Inc
 ATTN: M. Rosenblatt
 ATTN: K. Kreyenhagen

Calspan Corp
 ATTN: M. Holden

Dupont Chemical Corp
 ATTN: F. Bailey

Effects Technology, Inc
 ATTN: R. Parisse

General Electric Co, Space Division
 ATTN: C. Anderson
 ATTN: D. Edelman
 ATTN: G. Harrison

General Electric Co
Re-entry Systems Division
 ATTN: B. Maguire
 ATTN: P. Cline

DEPARTMENT OF DEFENSE CONTRACTORS (Continued)

General Research Corp
 ATTN: J. Mate

Harold Rosenbaum Associates, Inc
 ATTN: G. Weber

Hercules, Inc
 ATTN: P. McAllister

Institute for Defense Analyses
 ATTN: Classified Library
 ATTN: J. Bengston

Kaman Sciences Corp
 ATTN: F. Shelton
 ATTN: J. Keith
 ATTN: J. Harper
 ATTN: J. Hoffman
 ATTN: D. Sachs

Kaman Tempo
 ATTN: B. Gambill
 ATTN: DASIAC

Lockheed Missiles & Space Co, Inc
 ATTN: F. Borgardt

Lockheed Missiles & Space Co, Inc
 ATTN: R. Walz

Los Alamos Technical Associates, Inc
 ATTN: J. Kimmerly
 ATTN: P. Hughes

Martin Marietta Corp
 ATTN: E. Strauss

McDonnell Douglas Corp
 ATTN: R. Reck
 ATTN: H. Berkowitz
 ATTN: L. Cohen
 ATTN: D. Dean
 ATTN: E. Fitzgerald
 ATTN: P. Lewis, Jr.
 ATTN: J. Garibotti
 ATTN: G. Johnson
 ATTN: H. Hurwicz

McDonnell Douglas Corp
 ATTN: M. Potter

National Academy of Sciences
 ATTN: D. Groves
 ATTN: Medical Follow-up Agency

Pacific-Sierra Research Corp
 ATTN: G. Lang
 ATTN: H. Brode

PDA Engineering
 ATTN: J. McDonald
 ATTN: M. Sherman
 ATTN: J. Dunn

Physics International Co
 ATTN: J. Shea

DEPARTMENT OF DEFENSE CONTRACTORS (Continued)

R & D Associates

ATTN: P. Rausch
ATTN: W. Graham
ATTN: F. Field
ATTN: J. Carpenter

Rand Corp

ATTN: R. Rapp

Rockwell International Corp

ATTN: B. Schukin
ATTN: G. Perroue

Science Applications, Inc

ATTN: W. Plows
ATTN: W. Yengst
ATTN: J. Stoddard
ATTN: C. Lee
ATTN: J. Manship
ATTN: J. Warner

Science Applications, Inc

ATTN: W. Layson
ATTN: J. Cockayne

Science Applications, Inc

ATTN: A. Martellucci

Science Applications, Inc

ATTN: J. Burghart

Southern Research Institute

ATTN: C. Pears

SRI International

ATTN: H. Lindberg
ATTN: P. Dolan
ATTN: G. Abrahamson
ATTN: D. Curran

DEPARTMENT OF DEFENSE CONTRACTORS (Continued)

System Planning Corp

ATTN: F. Adelman

Systems, Science & Software, Inc

ATTN: G. Gurtman
ATTN: R. Duff

Terra Tek, Inc

ATTN: S. Green

Thiokol Corp

ATTN: J. Hinckman
ATTN: W. Shoun

TRW Defense & Space Sys Group

ATTN: P. Brandt
ATTN: D. Baer
ATTN: R. Plebisch
ATTN: N. Lipner
ATTN: A. Ambrosio
ATTN: A. Zimmerman
ATTN: T. Mazzola
ATTN: M. King
ATTN: W. Wood
ATTN: G. Arenguren
ATTN: R. Bacharach
ATTN: T. Williams
ATTN: M. Seizew
2 cy ATTN: I. Alber

TRW Defense & Space Sys Group

ATTN: E. Allen
ATTN: E. Wong
ATTN: L. Berger
ATTN: D. Kennedy
ATTN: D. Glenn
ATTN: W. Polich
ATTN: N. Guiles
ATTN: V. Blankinship
ATTN: P. Dal